Space Science Reviews manuscript No.
(will be inserted by the editor)

Using OpenGGCM to compute and separate magnetosphere magnetic perturbations measured on board low Earth orbiting satellites

J. Raeder · W. D. Cramer · K. Germaschewski · J. Jensen

received: March 28, 2016

Abstract We use Open Geospace General Circulation Model (OpenGGCM) simulations to predict magnetic field perturbations at Low Earth Orbiting (LEO) satellites such as SWARM, at high latitudes. The simulations allow us to separate three different major contributions to the observed perturbations, i.e., the perturbations caused by currents in the outer magnetosphere, field-aligned currents (FACs), and the currents flowing in the ionosphere. We find that at an altitude of 500 km the strongest contribution comes from FACs, followed by the perturbations caused by the ionospheric currents, while the magnetospheric currents make only a minor contribution. The high latitude perturbations do not average out over extended quiet time periods. There are significant variations in the patterns; however, on a large scale, the basic shape of the pattern remains stable. Thus, without

Physics Department & Space Science Center,
University of New Hampshire,
Durham, NH, 03824, USA
J.Raeder@unh.edu

explicitly removing the perturbations from the data, any spherical harmonics fit is expected to incur a bias. Although the predicted OpenGGCM perturbations do not compare particularly well with SWARM data, the simulations reproduce the overall pattern. However, they may still be useful to reduce the bias of the ensemble and produce better global spherical harmonic fits, by producing an ensemble whose external field contributions average out. Since this paper only scratches the surface of the role that models of the external field can play in producing unbiased internal field models, much progress is still possible, for example by improving the external model, investigating larger ensembles, and by considering data from geomagnetically disturbed times.

1 Introduction

Earth's magnetic field is created by numerous sources. Ampere's law states that currents generate the magnetic field. Such currents can be free currents or bound currents. The latter are microscopic and can be typically described as the magnetization of a material, such that $\mathbf{J}_\mathrm{M} = \nabla \times \mathbf{M}$, where $\mathbf{J}_\mathrm{M}$ is the magnetization current, and $\mathbf{M}$ the magnetization of the material.

As far as Earth's magnetic field is concerned, its contributions are usually divided into an internal part and into an external part. The internal part is due to currents in the Earth's core and the magnetization of rocks. Since the atmosphere is neither a conductor nor possesses any significant magnetization it does not contribute to the field. However, at high altitudes, the atmosphere becomes ionized and forms the ionosphere, which carries currents. At even larger distances from

the Earth, the magnetosphere is also made up of highly conducting plasma that carries significant currents.

The internal field is very stable and varies only on long time scales, i.e., longer than months.

Because the magnetic field is divergence free ($\nabla \cdot \mathbf{B} = 0$) and because there is neither a current nor any magnetization at the surface of the Earth ($\nabla \times \mathbf{B} = 0$), the field can be described as the gradient of a scalar magnetic potential Φ_{M}, i.e., $\mathbf{B} = -\nabla\Phi_{\mathrm{M}}$. Therefore, the internal part of the geomagnetic field is typically described in mathematical terms by an expansion of Φ_{M} in spherical harmonics (*Finlay et al.* 2010).

There are various ways to obtaining the expansion coefficients from data, which leads to different models. Typically, the models also include the time derivative of the coefficients, and thus of the field. This slow field change is also known as secular variation. The models also differ greatly as to the order of the expansion. Models with low expansion order ($\sim$10) mostly describe the core field. The crustal, i.e., magnetization field, has typically much higher wave number components and requires expansions of order 100 or more (see, for example: *Olsen et al.* 2006).

In contrast to the internal field, the external field is highly time variable. The currents in the magnetosphere and the ionosphere are mostly driven by the solar wind and the magnetic field carried by it, the Interplanetary Magnetic Field (IMF). The latter is variable on the order of seconds. However, the magnetosphere-ionosphere (MI) system acts to some extent as a low pass filter, i.e., fluctuations of frequencies larger than about a minute are either damped in the magnetosheath, reflected at the magnetopause, or reflected at the top side of the ionosphere. Thus, fluctuations seen on the ground and at Low Earth Orbiting (LEO) satellites typ-

ically show variability on a time scale of about a minute or larger. Besides those currents directly driven by the solar wind and IMF, other currents are induced in the ionosphere by the motion of the neutral atmosphere. These currents are typically much smaller than the ones induced by the magnetosphere. However, the currents driven by the magnetosphere occur mostly at high latitudes, i.e., the auroral zone. At low latitudes, the neutral wind driven currents, such as the equatorial electrojet, can dominate.

The high latitude currents are also highly variable on longer time scales. At times, the magnetosphere is geomagnetically quiet, causing only a low level of currents. Often, there is geomagnetic activity, which manifests itself in auroral displays and significant magnetic disturbances on the ground. A particular phenomenon of such activity is a substorm, which typically lasts a few hours (*McPherron et al.* 1973; *Baker et al.* 1996; *Lui* 1991; *Angelopoulos et al.* 2008).

Much stronger activity occurs during geomagnetic storms. These typically last a few days, and can in severe cases bring auroras to mid-latitudes (*McPherron* 1991). Such storms also cause strong distortions of the magnetic field observed on the ground that can reach magnitudes of $\sim$10% of the internal field. A typical example is the 'Bastille Day' storm of July 2000 (*Raeder et al.* 2001a,b; *Rastaetter et al.* 2005). In the magnetosphere literature any such deviations from a "baseline" are called "ground magnetic perturbations."

Although the external field emerging from the currents in the magnetosphere, the ionosphere, and the currents that couple the magnetosphere with the ionosphere is highly variable, it is not random. Thus, over long time scales (hours or longer), the external contributions do not average out, but show particular patterns (*Ijima and Potemra* 1976; *Weimer* 2001; *Anderson et al.* 2008), that can be

ordered to some extent by the clock angle and the magnitude of the IMF. Even during quiet times, the external ionosphere currents never vanish, and averaging over quiet time observations does not remove them (see, e.g. *Ritter et al.* 2004).

Geomagnetic activity is typically measured using indices. The storm disturbance index (Dst) is derived from low-latitude magnetometer stations and largely measures the energization of the ring current, a belt of hot plasma that circles the Earth between 3 and 7 R_E (Earth radii, a convenient length measure in magnetospheric physics). The indices AL, AU, AE are derived from stations at auroral latitudes. Specifically, the AL is the lower envelope of a number of stations at auroral latitudes, AU is the upper envelope, and AE is the difference. AL is a rough measure of the westward electrojet, AU of the eastward electrojet, and AE is a good measure of auroral activity. The premise of these indices is their ability to 'catch' substorms regardless of the local time at which they occur. This requires a dense and uniform (in longitude) coverage with stations, which is not often available. The Kp index is derived from mid-latitude stations. It mostly responds to storms, but less so to substorms, because the 3 hour cadence of the Kp index masks the weak "mid-latitude bay" ground magnetic signature that substorms produce at mid-latitudes. Note that storms and substorms are distinct processes (*Rostoker* 2000). It once was believed that storms are composed of substorms (*McPherron* 1997). However, it is now well established that substorms occur independently, although substorms can and do occur during storms. The frequency of storms is up to a few dozen per year during solar maximum, while substorms occur almost every day.

For the purpose of determining Earth's internal field, one must separate the internal from the external field contributions. With all measurements taken on the

ground, this is in principle easy and should fall right out of the spherical harmonics expansion. However, in practice, it is much more difficult, in particular, because the distribution of surface measurements is extremely uneven. Measurements from space using LEO satellites can provide a fairly uniform coverage. However, the price paid is that the ionosphere currents now appear as internal currents, and the expansion does not separate them, but rather lumps them into the internal field. Thus, the fitting of coefficients to the model then requires the proper removal of the ionosphere and magnetosphere contributions. In practice, only low-order contributions of the external field are removed (*Olsen et al.* 2006).

2 The OpenGGCM Model

The OpenGGCM is a global coupled model of Earth's magnetosphere, ionosphere, and thermosphere. The magnetosphere part solves the MHD equations as an initial-boundary-value problem. The MHD equations are only solved outside of ∼3 R_E of Earth. The region within 3 R_E is treated as a magnetosphere-ionosphere (MI) coupling region where physical processes that couple the magnetosphere to the ionosphere-thermosphere system are parameterized using simple models and relationships. The ionosphere-thermosphere system is modeled using the NOAA CTIM (Coupled Thermosphere Ionosphere Model) (*Fuller-Rowell et al.* 1996; *Raeder et al.* 2001a). In the following we describe each part of the model in more detail.

2.1 Outer Magnetosphere

The physics of the outer magnetosphere is governed by the magnetohydrodynamic equations, which we use in their normalized, semi-conservative form:

$$\frac{\partial \rho}{\partial t} = -\nabla \cdot (\rho \mathbf{v}) \tag{1}$$

$$\frac{\partial \rho \mathbf{v}}{\partial t} = -\nabla \cdot (\rho \mathbf{v}\mathbf{v} + p\mathsf{I}) + \mathbf{j}\times\mathbf{B} \tag{2}$$

$$\frac{\partial e}{\partial t} = -\nabla \cdot (\{e + p\}\mathbf{v}) + \mathbf{j} \cdot \mathbf{E} \tag{3}$$

$$\frac{\partial \mathbf{B}}{\partial t} = -\nabla\times\mathbf{E} \tag{4}$$

$$\nabla \cdot \mathbf{B} = 0 \tag{5}$$

$$\mathbf{E} = -\mathbf{v}\times\mathbf{B} + \eta\mathbf{j} \tag{6}$$

$$\mathbf{j} = \nabla\times\mathbf{B} \tag{7}$$

$$e = \frac{\rho v^2}{2} + \frac{p}{\gamma - 1} \tag{8}$$

Here, the symbols have their usual meaning, i.e., $\mathbf{B}$ and $\mathbf{E}$ are the magnetic and the electric field, respectively, $\mathbf{v}$ is the plasma velocity, ρ is the density, p is the pressure, $\mathbf{j}$ is the current density, η is a resistivity, I is the unit tensor, and γ is the ratio of specific heats of the plasma, assumed to be 5/3.

The semi-conservative formulation, which is mathematically equivalent to the either non-conservative (primitive variables) or fully conservative equations, is chosen because it allows for finite difference schemes that numerically conserve mass (ϱ), momentum ($\varrho\mathbf{v}$), and plasma energy (e), but with no numerical strict conservation of total energy (*Raeder* 2003). Fully conservative schemes that conserve total energy ($U = \frac{p}{\gamma-1} + \frac{\rho v^2}{2} + \frac{B^2}{2}$) often suffer from instability in low β regions where the pressure must be computed as the difference of two large quantities (U and $B^2/2$). Here, β is the ratio of plasma and magnetic field pressure. Such low β plasma occurs in the magnetosphere close to Earth and in the tail lobes. Counteracting such instability would make the model more diffusive, whereas using the

semi-conservative form of the equations only incurs significant errors at strong, low β shocks, which are untypical for the magnetosphere.

To solve the MHD equations in the outer magnetosphere we use an explicit second-order predictor-corrector finite difference time stepping scheme. The spatial derivatives are also computed using finite differences. However, because the simulation involves super-magnetosonic flows and shocks, simple finite differences are too dispersive, but flux-limited schemes must be used. In the case of the OpenGGCM, we use a hybrid scheme that was originally proposed by Harten (*Harten and Zwas* 1972), where we combine a fourth-order scheme with a minimal diffusion error (*Zalesak* 1979, 1981) with the diffusive first-order Rusanov scheme. The numerical switch produces a high-order solution in regions of smooth variation of the flow, i.e., where there are no discontinuities, such as shocks and contact discontinuities. Near such discontinuities, where the high-order scheme would fail due to numerical dispersion, a low order, less dispersive, but more diffusive, scheme is used. Such shock-capturing schemes are commonly used in computational fluid dynamics for the solution of trans-sonic and supersonic flows (*Hirsch* 1990; *Laney* 1998).

Maxwell's equation states that $\nabla \cdot \mathbf{B} = 0$ at all times, since there are no magnetic monopoles. Strictly speaking, this is only an initial condition for $\mathbf{B}$ because Faraday's law demands that if $\nabla \cdot \mathbf{B} = 0$ at some time, it is to remain so as the magnetic field evolves, which can be seen from:

$$\nabla \cdot \frac{\partial \mathbf{B}}{\partial t} = \frac{\partial (\nabla \cdot \mathbf{B})}{\partial t} = -\nabla \cdot \nabla \times \mathbf{E} = 0. \tag{9}$$

The accumulation of finite $\nabla \cdot \mathbf{B}$ can lead to serious errors, in particular spurious parallel acceleration, wrong magnetic topology (field lines that are not closed), and significant errors in the shock jumps (*Brackbill and Barnes* 1980; *Toth* 2000). There are a few methods to clean the magnetic field of monopoles, for example the projection method, but none of these is perfect, and they also incur substantial additional cost (*Toth* 2000). The OpenGGCM uses the Constrained Transport (CT) method introduced by Evans and Hawley (*Evans and Hawley* 1988), which employs a staggered grid that allows near perfect (to roundoff error) preservation of $\nabla \cdot \mathbf{B}$. With CT, the magnetic field components are put on cell faces, and the electric field components for the right hand side of Faraday's law are put on the centers of the cells' edges. Such staggered grids require interpolation for the coupling terms $\mathbf{j} \times \mathbf{B}$ and $\mathbf{j} \cdot \mathbf{E}$; however, this is a small price to pay for magnetic flux conservation.

An important aspect of every MHD code is the spatial grid. Many choices are possible, ranging from equidistant Cartesian grids to structured adaptive mesh refinement (AMR) grids (see *Raeder* 2003, for an overview and discussion of grids). The OpenGGCM employs a stretched Cartesian grid. Typically the grid extends to $\sim$20 R_E in the sunward direction, several 100 R_E in the anti-sunward direction (to the right), and $\sim$40 R_E in the transverse (y and z) directions. The grid resolution is typically 0.1-0.2 R_E at the sub-solar magnetopause and 0.2-0.3 R_E in the near-Earth tail, with a total of 10^7-10^8 grid cells.

The primary advantage of the OpenGGCM grid is that it allows for a well load balanced and efficient parallelized code, while it, for the most part, optimizes the resolution where it is needed. A uniform Cartesian grid would need 10^2-10^3 times the number of cells to achieve the same resolution in critical regions, such as the magnetopause or the plasma sheet. On the other hand, non-Cartesian or

AMR grids may be able to optimize resolution better, but they also incur a higher computational cost and require much more complex codes.

2.2 Ionosphere and MI Coupling

As outlined above, the MHD calculation only extends to $\sim$3 R_E from Earth. At that inner boundary the MHD part of the model is coupled with the ionosphere, mainly by the closure of field-aligned currents (FACs) in the ionosphere. The OpenGGCM uses a static dipole model to map the FACs into the ionosphere, which is possible for two reasons: (1) the current density obeys a continuity equation and (2) these currents typically do not close across field lines at this altitude. At the ionosphere end, a potential equation is solved on a sphere (or a section thereof) to yield the ionospheric convection potential (*Vasyliunas* 1970; *Wolf* 1983; *Fedder and Lyon* 1987; *Vasyliunas* 1988). The potential is then mapped back to the inner boundary of the MHD calculation where it is used as boundary condition for the flow and field integration ($\mathbf{v} = (-\nabla\Phi)\times\mathbf{B}/|B|^2$). Because the mapping originates at 3 R_E, it covers the latitudes from $\sim$55° to 90°. At the ionosphere end of the model the MHD solver is coupled to the Coupled Thermosphere-Ionosphere Model (CTIM). CTIM is described in detail elsewhere (see *Fuller-Rowell et al.* 1996, and references therein); thus we only provide a brief description here. CTIM is a global multi-fluid model of the thermosphere-ionosphere system with a long heritage. CTIM solves both neutral and ion fluid equations self-consistently from 80 to 500 km for the neutral atmosphere and from 80 to 10,000 km for the ionosphere on a spherical grid with 2° latitude resolution and 18° longitude resolution. The thermosphere part solves the continuity equation, horizontal momentum equation,

energy equation, and composition equations for the major species O, O_2, and N_2 on 15 pressure levels. The ionosphere model part solves the continuity equations, ion temperature equation, vertical diffusion equations, and horizontal transport for H^+ and O^+, while chemical equilibrium is assumed for N_2^+, O_2^+, NO^+, and N^+. The horizontal ion motion is governed by the magnetospheric electric field. The coupled model includes about 30 different chemical and photo-chemical reactions between the species. Compared to the magnetosphere, the CTIM time scales are relatively long, allowing for numerical time steps of the order of one minute. Consequently, CTIM is computationally very efficient and runs considerably faster than real-time (>10 times) on a single CPU.

CTIM's primary input are the solar UV and EUV flux (parameterized by the solar 10.7 cm radio flux), the tidal modes (forcing from below), auroral electron precipitation parameters, and the magnetospheric potential, from which it calculates the electric field.

The electron precipitation parameters, energy flux F_E, and mean energy E_0 are computed separately for diffuse precipitation and for discrete precipitation, i.e., for electrons accelerated in regions of upward FAC.

Diffuse precipitation is parameterized by:

$$F_E = n_e(kT_e/2\pi m_e)^{\frac{1}{2}} \qquad , \qquad E_0 = kT_e, \tag{10}$$

where T_e and n_e are the magnetospheric electron temperature and density, respectively, and k is the Boltzmann constant.

Discrete electron precipitation is modeled using the Knight relation (*Knight* 1972):

$$\Delta\Phi = K^{-1}\max(0, -j_\parallel) \tag{11}$$

$$K = \frac{e^2 n_e}{\sqrt{2\pi m_e k T_e}}, \tag{12}$$

$$F_E = \Delta\Phi_{\parallel} j_{\parallel} \qquad , \qquad E_0 = e\Delta\Phi_{\parallel}, \tag{13}$$

where $\Delta\Phi$ is the parallel potential drop on an auroral field line, and $j_{\parallel}$ is the field aligned current, with the convention that a positive $j_{\parallel}$ is downward current. Because the MHD model cannot provide an electron temperature, we use the MHD single fluid temperature adjusted by a tunable adjustment factor.

The electric field in the ionosphere is assumed to be a potential field and is obtained from current conservation, which leads to the following potential equation (*Vasyliunas* 1970; *Kelley* 1989):

$$\nabla \cdot (\Sigma \cdot \nabla\Phi) = -j_{\parallel} \sin I \tag{14}$$

with the boundary condition Φ=0 at the magnetic equator. Because the ionosphere is a magnetized and partially ionized plasma, the ionospheric conductance is a tensor (*Strangeway and Raeder* 2001), given by:

$$\Sigma = \begin{pmatrix} \Sigma_{\theta\theta} & \Sigma_{\theta\lambda} \\ -\Sigma_{\theta\lambda} & \Sigma_{\lambda\lambda} \end{pmatrix} \tag{15}$$

$$\Sigma_{\theta\theta} = \frac{\Sigma_P}{\sin^2 I} \quad , \quad \Sigma_{\theta\lambda} = \frac{\Sigma_H}{\sin I} \quad , \quad \Sigma_{\lambda\lambda} = \Sigma_P, \tag{16}$$

where Σ_H is the Hall conductance, Σ_P is the Pedersen conductance, θ is the magnetic latitude, λ is the magnetic longitude, and I is the magnetic field inclination.

The ionospheric Hall and Pedersen conductances are computed by CTIM from first principles, i.e., from the electron-neutral collision terms. In addition, the neutral wind dynamo is explicitly included in the solution of the electric potential. The neutral dynamo plays no significant role during substorms, but can produce a flywheel effect during storms, where the neutrals are accelerated by ion drag during

the storm main phase, while the neutrals impart momentum on the ions during the recovery phase and thereby generate an electric field (*Rishbeth et al.* 1991). Using the CTIM conductances, as opposed to using conductances from empirical models, significantly affects the simulations. The effect of different conductance models in the OpenGGCM and its predecessors has been studied previously (*Raeder et al.* 1996, 2001a). The latter study showed that the model produced significantly more realistic ionosphere potentials in runs where the MHD model was coupled with CTIM.

Figure 1 shows a block diagram of the OpenGGCM elements and their relationships. The connection arrows indicate the flow of data. Note that the OpenGGCM only requires a minimal set of inputs. The solar wind and IMF are typically taken from a solar wind monitor such as ACE, Wind, or the merged OMNI data set. The SW and IMF data need to be known over the entire inflow boundary. We thus need to make an assumption how the solar wind is structured. One option is to assume that the solar wind parameters are independent of Y_{GSE} and Z_{GSE}. In that case, the IMF B_x component cannot change in time because that would violate $\nabla \cdot \mathbf{B} = 0$. If there are significant IMF B_x variations, the assumption of Y_{GSE} and Z_{GSE} independence cannot be true. In that case, we attempt to find a direction $\mathbf{N}$ in the solar wind such that the magnetic field component along that direction (B_N) does not change significantly. Since usually only one solar wind monitor is available, we employ the minimum variance method of *Sonnerup and Cahill* [1967, 1968] to find that direction. We call this the MINVAR method. If observations from multiple solar wind monitors are available, more precise methods are available (see, for example *Russell et al.* 2001). If B_N is fairly constant over the time interval of interest, we set B_N to be constant in time at the value of

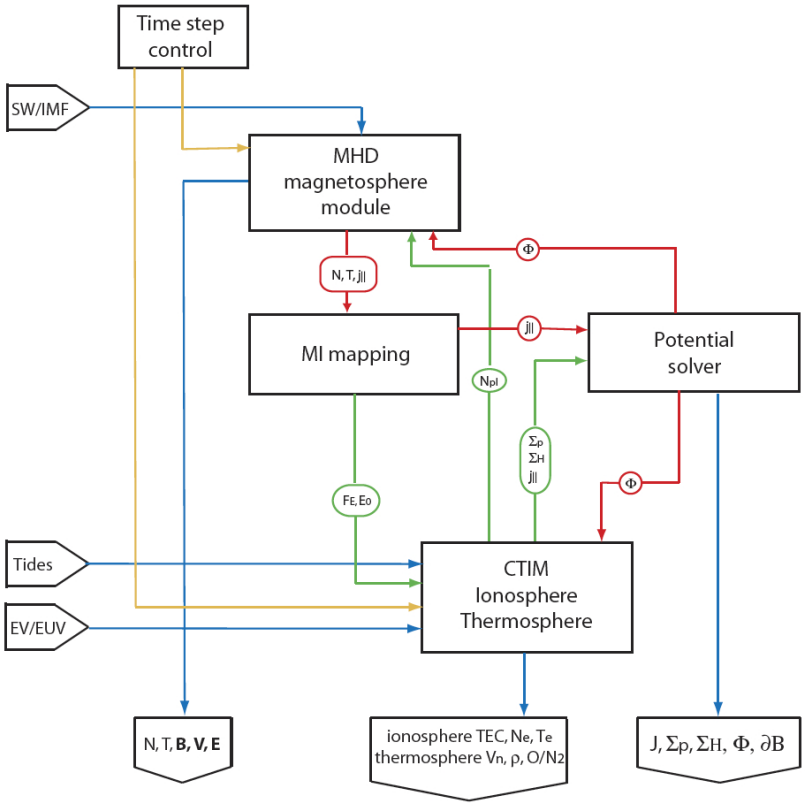

Fig. 1 Block diagram of the OpenGGCM with its models and with data/control flow. Blue lines denote model input and output. Red lines denote data flow with strong coupling. Green lines denote data flow with weak or slow coupling. Orange lines denote control flow. B, N, and T are the magnetospheric magnetic field, plasma density, and temperature, respectively. The field aligned current is $j_{\parallel}$, Φ is the ionosphere potential, F_E and E_0 the energy flux and mean energy of precipitating electrons, Σ_H and Σ_P the ionosphere Hall and Pederesen conductances, and ∂B is the ground magnetic perturbation.

its average and then transform the field back into GSE coordinates and use it as input to the MHD model. In this case the solar wind and IMF convects into the model as sheets whose orientation is given by their normal vector **N**.

In the case that B_N from the minimum variance transform is not nearly uniform (defined such that the variance of B_N is significantly smaller, say <10 % of the total field) the solar wind does not have a simple sheet-like structure and there is also not enough information available to determine the structure. The options are to either ignore the IMF B_x component or to set it to some constant value that seems reasonable. This may in many cases not be a bad choice, because the IMF B_x component essentially does not contribute to the interplanetary electric field (IEF) and because the draping of the IMF around the magnetosphere normally reduces the B_x component before the field interacts with the magnetosphere. However, if the IMF B_x component dominates the IMF it may affect the reconnection geometry at the magnetopause and the simulation results must be carefully assessed for their validity. In the test case presented below, we simply set B_x to zero, because it was small throughout the interval.

The OpenGGCM has been used to investigate a variety of magnetosphere phenomena, such as Flux Transfer Events (*Berchem et al.* 1995; *Raeder* 2006), substorms (*Raeder et al.* 1998; *Ge et al.* 2011), ballooning modes (*Raeder et al.* 2010; *Zhu et al.* 2013; *Raeder et al.* 2012), magnetopause reconnection (*Raeder et al.* 2000; *Le et al.* 2001; *Li et al.* 2008, 2009; *Dorelli et al.* 2007), field-aligned currents (*Vennerstrom et al.* 2005, 2006; *Moretto et al.* 2006), and Poynting flux into the ionosphere (*Li et al.* 2011).

Since the OpenGGCM is a community model housed at the Community Coordinated Modeling Center (CCMC), there have also been a number of evaluation and metrics studies been conducted by CCMC personnel (*Pulkkinen et al.* 2011, 2013; *Rastatter et al.* 2013).

3 Calculation of Magnetic Field Perturbations

OpenGGCM computes the magnetic field, and thus the current density in the outer magnetosphere. The values are gridded on a Cartesian non-equidistant grid (*Raeder* 2003). The grid is designed to maximize resolution near the Earth, at the dayside magnetopause, and in the near-Earth plasma sheet, where it matters most. The resolution in these regions is typically of the order of 0.2-0.03 R_E. The outer magnetosphere is the region above R_o geocentric distance, where R_o is chosen here to be 4.5 R_E. In the following, this region, where the current density is $\mathbf{j}_{\rm MAG}$, is designated as 'MAG'. Field-aligned currents (FACs) are calculated in the magnetosphere at a distance of $R_{\rm FAC}$ and mapped into the ionosphere, which is considered a two-dimensional spherical shell at an altitude of $R_{\rm IO}$ = 110 km. This defines the region 'FAC', between 110 km and R_o, where only FAC flows. Its direction is along dipole field lines, and the magnitude is scaled by flux tube cross section, i.e.:

$$\mathbf{j}_{\rm FAC}(\mathbf{x}) = j_{\rm FAC}(110{\rm km})\frac{\mathbf{B}_{\rm DIP}(\mathbf{x})}{B_{\rm DIP}(\mathbf{x})}\frac{B_{\rm DIP}(\mathbf{x})}{B_{\rm DIP}(110{\rm km})} \tag{17}$$

In the ionosphere, the current density is $\mathbf{j}_{\rm CIO}$, which is a spherical shell current sheet. It is calculated by first solving for the ionosphere potential, and then using Ohm's law with the ionosphere conductance (*Raeder et al.* 2001a; *Raeder* 2003; *Raeder et al.* 2008). Variables associated with this current are labeled with 'CIO'.

At any given point $\mathbf{x}$ the magnetic perturbation is calculated using Biot-Savart law:

$$\delta\mathbf{B}(\mathbf{x}) = \frac{\mu_0}{4\pi}\int_V \mathbf{j}_{\{\rm MAG,FAC,CIO\}}\times\frac{\mathbf{x}-\mathbf{x}'}{|\mathbf{x}-\mathbf{x}'|^3}d^3x' \tag{18}$$

Because the integrand falls off very quickly, the integrals do not need to extend over all space. If $\mathbf{x}$ lies in a plane at 500 km altitude, we integrate $\mathbf{j}_{\mathrm{MAG}}$ up to 40,000 km distance. Note, that for this integral all currents lie outside of the observation points, and we need not be concerned about a diverging integrand. The integral is performed as a simple Riemann sum. Any higher order integration formula would not make sense, because one would have to interpolate (linearly, to avoid artificial extrema) the current density, which would negate the benefits of higher order integration.

The $\mathbf{j}_{\mathrm{CIO}}$ integral extends only over a two-dimensional manifold and is also calculated as a Riemann sum, this time as a sum over $R_{\mathrm{IO}}^2 \sin\theta' d\theta' d\phi'$ area elements. For this integral, the currents are also outside the observation point, so there is no concern of the integrand diverging.

The integral associated with $\mathbf{j}_{\mathrm{FAC}}$ is more difficult to calculate, because the observation point is immersed in the current. There is a certain distance r_1 from the observation point within which $\mathbf{j}_{\mathrm{FAC}}$ can be considered constant. This distance is basically given by the grid resolution at which $\mathbf{j}_{\mathrm{FAC}}$ is stored. We choose r_1=1 km, which is very conservative. The Biot-Savart integral is then computed as a Riemann sum over spherical volume elements $r'^2 \sin\theta' dr' d\phi' d\theta'$, starting at r_1, and with dr' increasing geometrically stepping outward. The summation is terminated when all of the FAC volume is included. The parameters r_1, $d\phi'$, $d\theta'$, and $dr'(r')$ are determined by convergence tests to find an optimal trade-off between accuracy and computational cost.

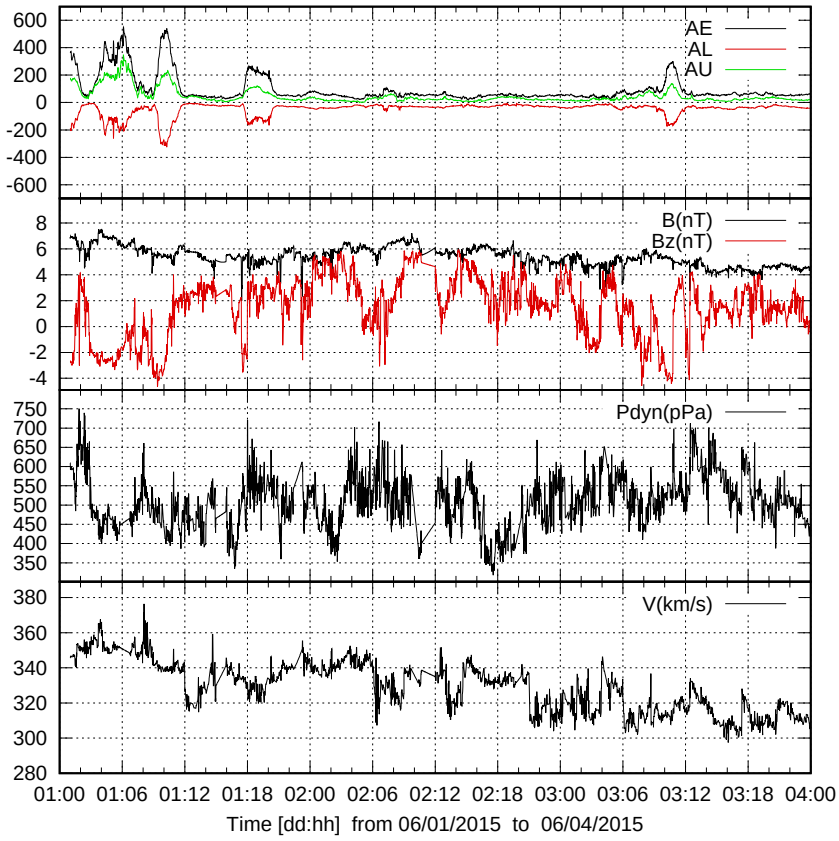

Fig. 2 Solar wind, IMF, and geomagnetic activity between 2015-06-01 and 2015-06-04. The figure shows, from top to bottom the geomagnetic indices AL, AU, and AE, the IMF B_z and magnitude, the dynamic pressure, and the solar wind speed. During the period from 2015-06-01 2200 UT to 2015-06-03 0600 UT the magnetosphere is quiet, while the IMF B_z component is mostly northward, and both the solar wind speed and its dynamic pressure is comparatively low.

4 Perturbation Maps

In order to estimate the "pollution" that the external currents cause, we picked a particularly quiet day and ran OpenGGCM simulations for that event. Figure 2 shows solar wind and IMF data, along with AL, AU, and AE indices for the

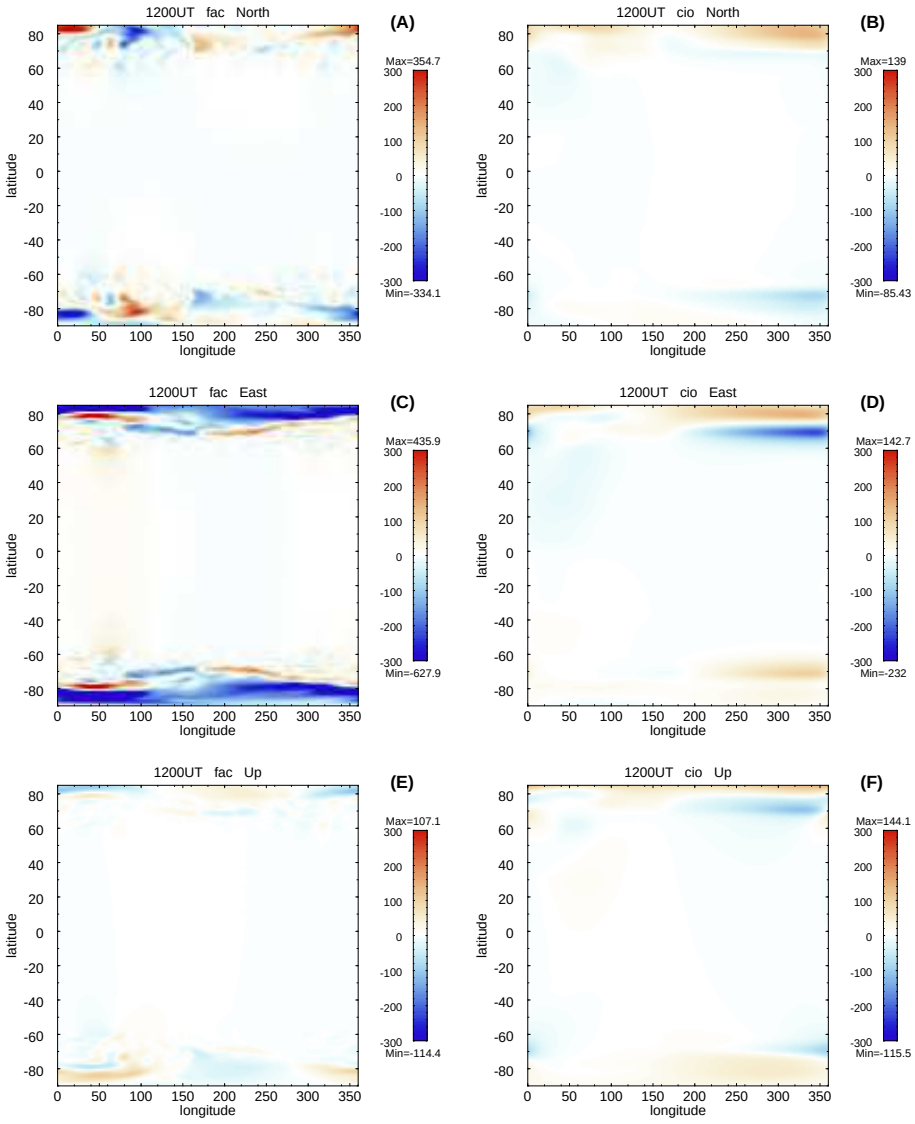

Fig. 3 Latitude-longitude maps of the magnetic field perturbation at 500 km altitude. The left column shows the perturbations due to field-aligned currents. The right column shows the perturbations due to ionospheric currents. The top row shows the north-south perturbations, the middle row shows the east-west perturbations, and the bottom row shows the radial perturbations. The color scale is the same in all panels to illustrate the much smaller radial perturbations compared to the other two.

period 2015-06-01 through 2015-06-03. The indices show some activity on June 1, and then again on June 3. However, June 2, 2015 is a very quiet day, during which AE never exceeds ∼70 nT. The solar wind speed is low, around 320-340 km/s, which is typical slow solar wind for this solar cycle, and so is the solar wind dynamic pressure, between 400 and 600 pPa, where typical values are around 1400 pPa. As expected for a quiet day, the IMF magnitude is small, and the clock angle is northward, i.e., the sign of B_z is positive.

While the magnetic field perturbations in the polar regions can easily be spotted in the data because of their high-frequency content (see below), the observations do not provide a global picture of the perturbations. Even though the model predictions have limitations, the model can provide a global overview of the perturbations. Furthermore, with the model it is possible to separate the different contributions. As outlined above, we consider the contributions from the outer magnetosphere, the field-aligned currents, and the ionosphere currents.

Figure 3 shows the three field components of the FACs (left column) and of the ionosphere currents (right column). From top to bottom, the panels show the north component, the east component, and the radial component, of the field. For better comparison, we kept the scale the same for all plots, i.e., at ±300 nT. As expected, because of the nature of these currents, the perturbations dominate at high latitudes, i.e., above ±65 degrees. The FAC contribution is substantially stronger than the ionosphere contribution. Also, the north and the east components are stronger than the radial components. This is easy to understand for the FAC contribution, since the FAC flows mostly radial, and thus by virtue of Biot-Savart's law should not produce a radial field component. The ionosphere currents flow in a spherical shell at 110 km altitude. These currents could well produce a radial component.

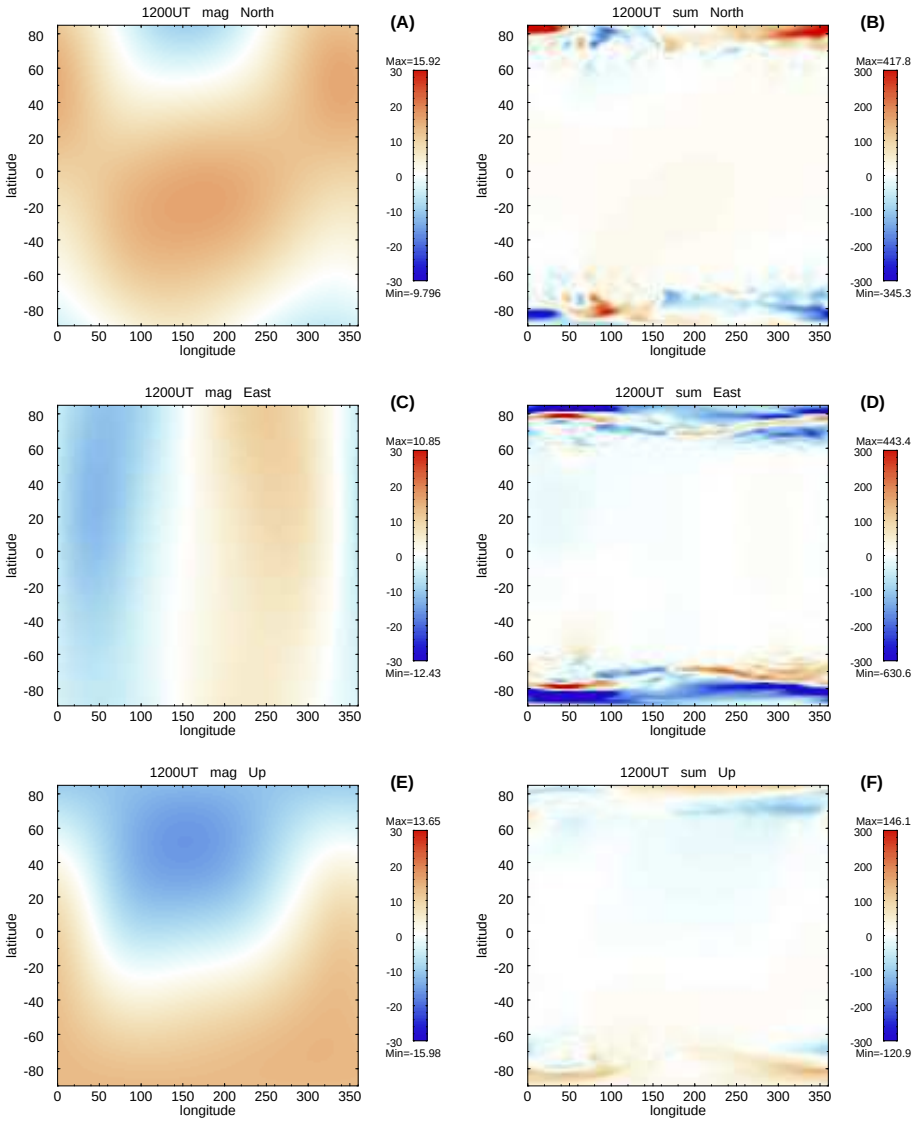

Fig. 4 Latitude-longitude maps of the magnetic field perturbation at 500 km altitude in the same format as Figure 3, except that the left column shows the perturbations due to the outer magnetosphere, and the sum of all perturbations is shown on the right side. The color scale for the magnetosphere perturbations is narrower by a factor 10, because these perturbations are much smaller than the others.

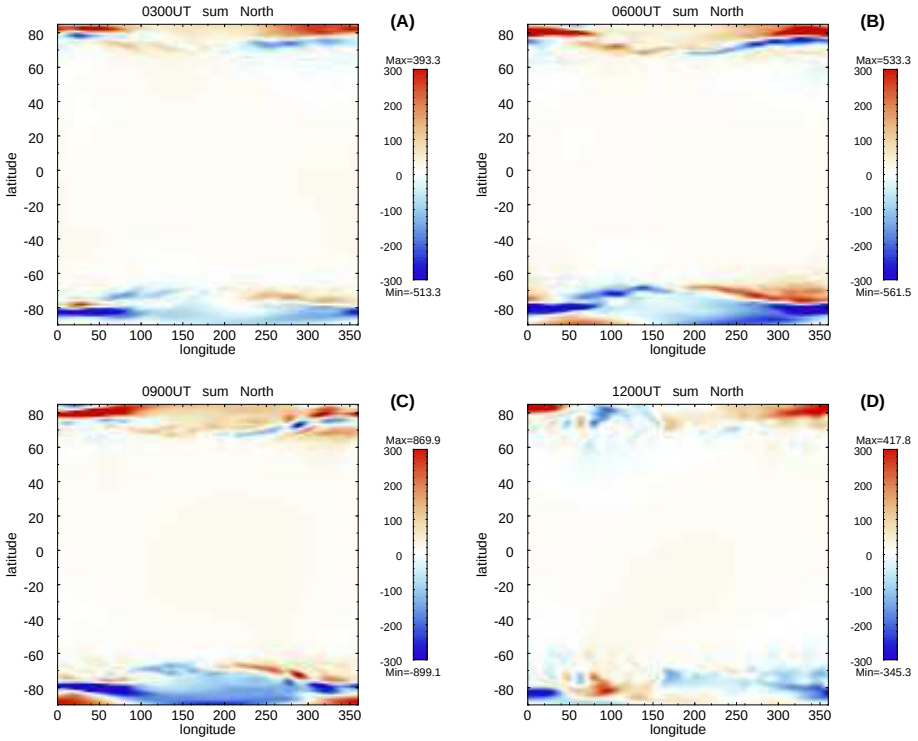

Fig. 5 Maps of the northward component of the total field perturbation at 500 km altitude at 4 different time, 3 hours apart. The overall pattern of the perturbation does not change very much over time.

Such a signal would be expected to be strong if the ionosphere currents flowed in circular loops that have roughly the same dimensions as the distance to the spacecraft, i.e, ∼400 km. Apparently, such current loops are not a major component of the ionosphere currents. Since the ionospheric Pedersen currents provide the closure for the FAC (*Vasyliunas* 1970; *Wolf* 1983; *Vasyliunas* 1988), they are by definition not closed loops, and thus do not produce a significant radial field component. Hall currents, on the other hand, are closing with themselves, by definition (*Kelley* 1989), and could thus produce radial fields. However, judging from the plots, the Hall currents must be small or widely dispersed.

Figure 4 shows, in the same fashion as Figure 3, the outer magnetosphere contribution on the left column, and the sum of all contributions on the right. Since the magnetosphere contribution comes from currents that are far away, they are much less structured. Still, patterns are discernible, such that the north component is almost uniformly positive. This may be the result of the superposition of the dayside magnetopause currents (also known as Chapman-Ferraro currents) and the ring current. Since this is a quiet period, the ring current contribution (which is negative) is small, so that the magnetopause contribution (which is positive on the Earth's surface) dominates. This is consistent with the fact that during quiet times the Dst index, which is derived from the north component measured by four equatorial magnetometers, tends to be positive.

The total field, in the auroral zone, is highly structured, as seen in the right panel of Figure 4. This makes it difficult for the model to predict satellite passes correctly because a small shift in the pattern can cause a large change of the predicted perturbation at the satellite location. It is important to note, however, that the basic shape of the pattern does not change much in time.

Figure 5 demonstrates this. It shows the northward components at four different times, with three hours time between panels. The large scale patterns stays fairly constant, although there are some changes in the solar wind and IMF (see Figure 2.) Thus, these perturbations will not average out, but are expected to create a bias when spherical harmonics are fitted to the data without corrections.

5 Test Case

In order to estimate the realism of the simulations, we compare our simulations with SWARM data for that event, by calculating the perturbations along the SWARM track. We use geographic (GEO) spherical coordinates throughout, i.e., the field has the components B_r (radial, denoted with *er* in the plots), B_θ (northward, denoted with *et*), and B_φ (eastward, denoted with *ep*).

As expected, the simulations are far from perfect. Figure 6 shows a pass over the northern polar cap by SWARM A around 1100 UT. The contribution from the different current systems are shown separately, along with their sum, which is the predicted signal. The perturbations seen by SWARM are fairly irregular and do not follow the typical region-1 (R1) / region 2 (R2) current pattern. This is not surprising, because the IMF is weak and mostly northward. The pattern from the simulation is also not that of a typical R1/R2 signature. It follows the observed pattern more or less in general terms, but lacks the high frequency components seen in the SWARM data. This is obviously due to the limited resolution of the model. The minima and maxima of the model prediction roughly match the observation; however, the model also shows extrema that are not in the data, such as the maximum in the north and east components around 1102 UT. It is also obvious from the figure that the model overestimates the magnitude of the perturbations.

Comparison of the three different perturbations shows that the FAC perturbation (fac, green lines) dominates. This is expected, because the satellite crosses right through the FAC current sheets. Next in magnitude are the perturbations originating from ionosphere currents (*cio*, yellow lines). These currents are assumed to flow at 110 km altitude, i.e., in the E region, and are thus at least 400

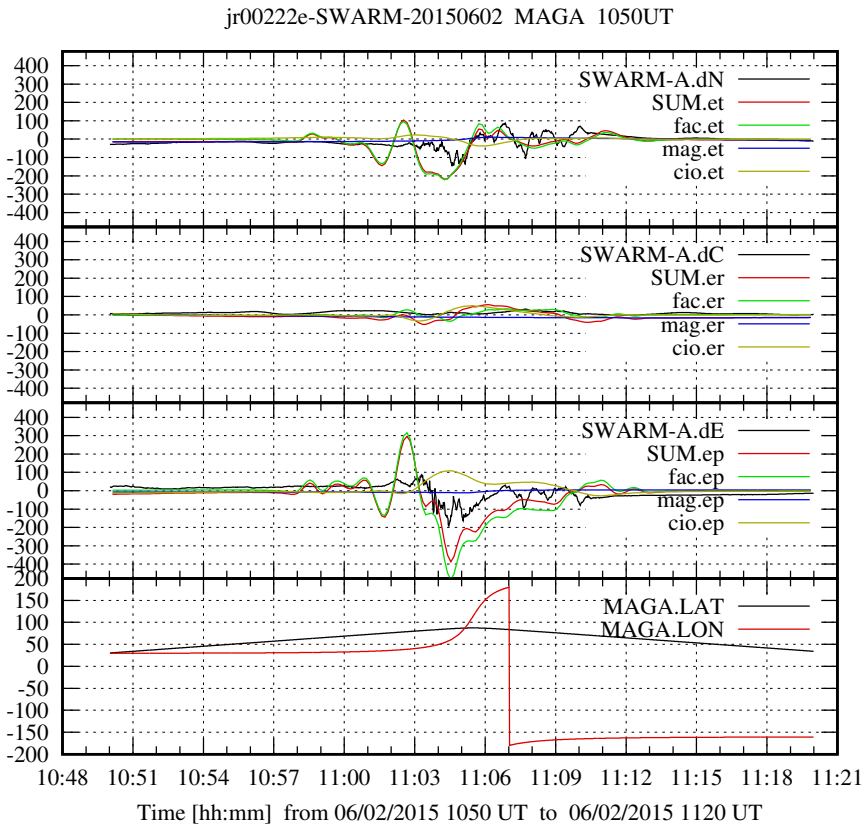

Fig. 6 Comparison between SWARM A observations and corresponding OpenGGCM predictions. The top three panels show the north, radial, and east components, respectively. Each of the panels shows the contributions due to Field Aligned Currents (fac), due to currents flowing in the outer magnetosphere beyond 4.5 R_E , and the contribution from currents flowing in the ionosphere (cio). SUM denotes the sum of these contributions, i.e., the expected signal. The bottom panel shows the latitude and longitude of the SWARM A track.

km away from the spacecraft. Because of that distance, the perturbations from these currents are also smoother, i.e., they have longer wavelengths than the FAC induced perturbations. The perturbations due to magnetosphere currents (*mag*,

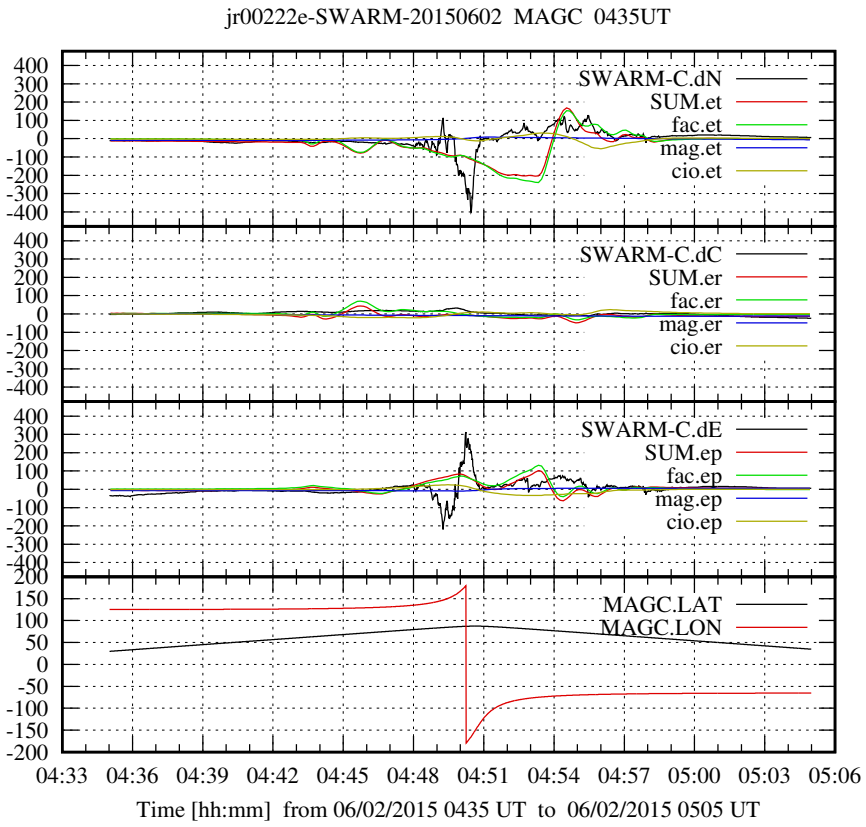

Fig. 7 Comparison between SWARM C observations and corresponding OpenGGCM predictions during the northern polar cap crossing around 0450 UT. The panels show the same quantities as Figure 6.

blue) are at least 4.5 R_E from the spacecraft and show thus even less structure. They are also much weaker than the other perturbations.

Figure 7 shows another example of a polar cap crossing. Here again the simulation predicts the patterns to some extent, but in contrast to Figure 6, the model underpredicts the magnitude of the perturbations. Like in the previous case, the radial perturbations are much smaller than the north and east perturbations. This is due to the fact that the FACs flow almost radially and thus, by virtue of Am-

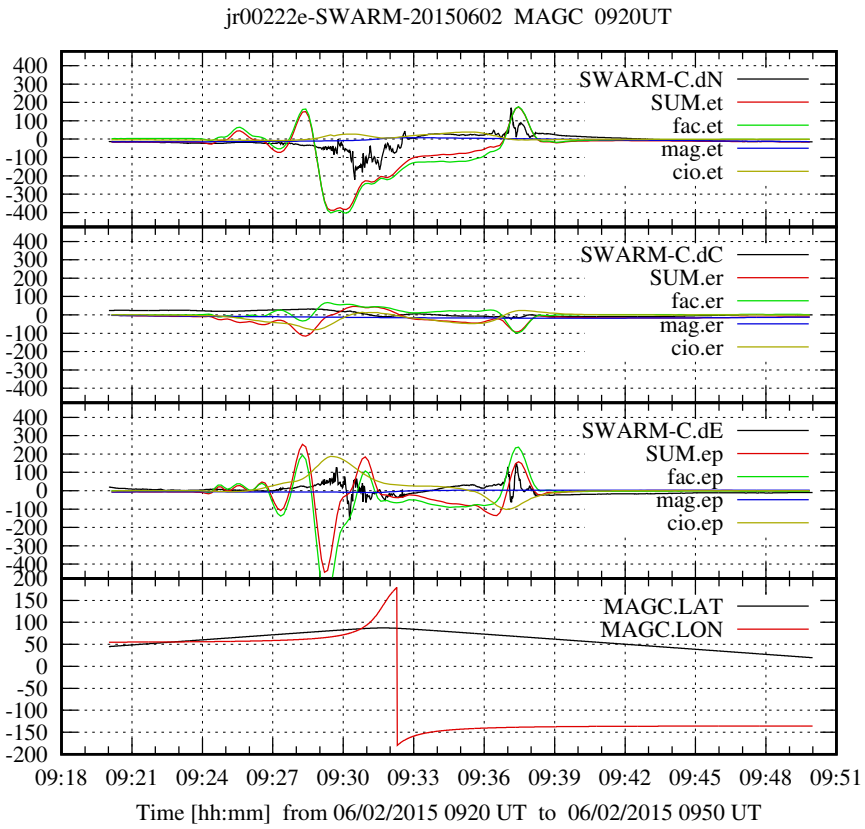

Fig. 8 Comparison between SWARM C observations and corresponding OpenGGCM predictions during the northern polar cap crossing around 0930 UT. The panels show the same quantities as Figure 6.

peres law, should not produce a radial component. There is still a radial component because the FACs are not exactly radial, and because of the other currents.

Figure 8 shows an example where the model almost completely fails. Compared to the other cases the polar cap is wider at this time. Although the modeled perturbations are roughly in the right place, their magnitudes are too large by a factor 2-4.

The tendency of the model to overpredict the observed perturbations is fairly universal, i.e., it also occurs in many of the passes from the same simulation that are not shown here. This may be due to multiple reasons, such as limited resolution or reconnection rates that are too high. However, the model generally produces polar cap potentials that are reasonable. Thus, ionosphere conductances, which in turn depend on auroral precipitation, at least in the night side, are likely the culprit.

6 Discussion

We have computed OpenGGCM simulations of a geomagnetic quiet day in order to separate the contributions from different external current systems. We also compared the resulting magnetic field perturbation along the SWARM satellite tracks with the actual data. Clearly, the model cannot predict the observations with sufficient accuracy such that one could just simply subtract the simulated predictions from the data to remove the effects created by the external current systems. However, the simulations show, as do empirical models (*Weimer* 2001; *Anderson et al.* 2008), that even when the solar wind and the IMF are not constant, the perturbation pattern does not vary very much. Thus, any fitting procedure that relies on the fact that the perturbations during geomagnetic quiet days are not only small, but may also average out, will likely incur a bias.

Similar conclusions were reached by *Olsen and Stolle* (2016, this issue). They used an empirically obtained FAC pattern, from which they extrapolated a complete three-dimensional closed current system. From that, they computed the perturbations at the 450 km level, very similar to what we presented here. They did

not, however, differentiate the contributions from different sources. Their results, presented in Figure 8 of their paper, may be directly compared to the right panel of Figure 4. Similar to our findings, the latitudinal and longitudinal perturbations are largest, and the radial component is significantly smaller. The magnitude of the perturbations in their analysis are smaller than in ours, but on the flip side, their perturbation patterns are substantially smoother than ours as well. This is due to the smooth FAC pattern that they use. This indicates that the total integrated FAC in their model is probably similar to that in our model, but has a smoother distribution. In other words, their FAC pattern lacks the smaller scale perturbations that are present both in our simulations, and typically are also present in the data. Consequently, the peak FAC densities are larger in our model, as are the resulting perturbations. That is particularly true for the FAC part, because that part is directly proportional to the FAC current density, whereas the CIO and MAG parts are sensitive to the total current in the entire system.

Although it is apparently too much to expect from the model to reproduce the observed perturbations pass-by-pass, the model might still be useful to eliminate the bias induced by the external field contributions. If one subtracted the predicted model perturbations from the data, the corrected data would still exhibit a net external contribution for any given pass. However, over the average of many passes, that contribution may average to a hopefully much smaller bias than without such correction. In other words, if $\delta\mathbf{B}_{\mathrm{model}}(\mathbf{x})$ is the modeled perturbation and $\delta\mathbf{B}_{\mathrm{true}}(\mathbf{x})$ is the true perturbation, then $| < \delta\mathbf{B}_{\mathrm{true}}(\mathbf{x}) - \delta\mathbf{B}_{\mathrm{model}}(\mathbf{x}) > |$ should be smaller than $| < \delta\mathbf{B}_{\mathrm{true}}(\mathbf{x}) > |$ alone, where the averaging $< ... >$ is over many passes and $|...|$ is an appropriate norm. Because $\delta\mathbf{B}_{\mathrm{true}}(\mathbf{x})$ is not random, its effects do not average out in the process of spherical harmonics (SPH) coefficient estimation.

On the other hand, $\delta\mathbf{B}_{\rm true}(\mathbf{x}) - \delta\mathbf{B}_{\rm model}(\mathbf{x})$ may be much closer to randomness (ideally obeying a Gaussian distribution), such that the errors would average out much better.

Judging from the results above, the model mostly overpredicts the observed perturbations. This might introduce a bias in the opposite direction that is worse, which may, however, be corrected by scaling the model results appropriately.

Using the model predictions to remove external field contributions from the data may also allow to expand the amount of data included in the fitting. At present, data from geomagnetically active times are generally not used for fitting because of the external contributions. However, during active times, the FACs, and thus the ionosphere currents and the perturbations are often better defined than during quiet periods; i.e., the FACs form a well defined R1/R2 current system, which may be better predictable than currents during quiet times. Since quiet times are comparatively rare, using data during moderately active times could substantially expand the database that can be used for fitting.

There is, of course, also substantial room to improve the model. For example, the model conductances depend, in particular in the night side, on electron precipitation. The model computes the electron precipitation parameters F_E (energy flux) and E_0 (mean energy) using fairly simple parameterizations. These parameterizations, which depend on a number of free parameters, could certainly be improved.

7 Summary

We used OpenGGCM simulations to predict magnetic field perturbations at LEO satellites such as SWARM. The simulations allow to separate three different contributions to the observed perturbations: (a) from currents in the outer magnetosphere, (b) from field-aligned currents, and (c) from the currents flowing in the ionosphere. We find that:

1. The strongest contribution comes from FACs. This contribution also has the highest spatial frequency, because the spacecraft traverse the highly structured current sheets.
2. The ionospheric currents also produce strong contributions at the satellites' altitude of about 500 km. Since these current are remote, they cause perturbations with spatial wavelengths that are comparable to the spacecraft distance from the currents, i.e., a few hundred km.
3. The currents in the magnetosphere (defined by a distance larger than 4.5 R_E from the Earth center) cause much smaller contributions. Also, because these currents are farthest for the observation points, their field perturbations should only affect the lowest order coefficients of a spherical expansion.
4. Even over an extended quiet time period, the perturbations do not average out. There are significant variations in the patterns; however, on a large scale, the basic shape of the pattern remains stable. Thus, without explicitly removing the perturbations from the data, any spherical harmonics fit will incur a bias.
5. The predicted OpenGGCM perturbations do not compare well with SWARM data. Although the location of the perturbation is a fairly good match, the predicted perturbations are often larger by a factor 2-3, although there are also

times when they are smaller. The model also does not reproduce the highest frequencies seen in the data, due to insufficient resolution. Predictions might be improved by better precipitation models, or by better numerical resolution.

6. Even though the OpenGGCM predictions are not as good as one may wish, they may still be useful to reduce the bias of the ensemble. This will require further investigation.

Obviously, this paper only scratches the surface of the possible role that global magnetosphere-ionosphere-thermosphere simulations can play in improving internal field models. So far we only considered quiet times, and only one particular day. Future research should address ensembles, geomagnetically perturbed times, and practical attempts to remove the bias introduced by external sources.

Acknowledgements The authors would like to thank the conveners of the ISSI workshop *Earth Magnetic Field: Understanding Sources from the Earth's Interior and its Environment* Claudia Stolle, Nils Olsen, Art Richmond, and Hermann Opgenoorth, who inspired this research. The work at UNH was funded through grant AGS-1143895 from the National Science Foundation, and NASA/LWS grant NNX13AK31G. Computations were performed on Trillian, a Cray XE6m-200 supercomputer at UNH supported by the NSF MRI program under grant PHY-1229408.

References

Anderson, B. J., H. Korth, C. L. Waters, D. L. Green, and P. Stauning, Statistical birkeland current distributions from magnetic field observations by the iridium constellation, *Annales Geophysicae*, *26*, 671–687, 2008.

Angelopoulos, V., et al., Tail reconnection triggering substorm onset, *Science*, *321*, 931, 2008.

Baker, D. N., T. I. Pulkkinen, V. Angelopoulos, W. Baumjohann, and R. L. McPherron, Neutral line model of substorms: Past results and present view, *J. Geophys. Res.*, *101*, 12,975, 1996.

Berchem, J., J. Raeder, and M. Ashour-Abdalla, Magnetic flux ropes at the high – latitude magnetopause, *Geophys. Res. Lett.*, *22*, 1189, 1995.

Brackbill, J. U., and D. C. Barnes, The effect of nonzero div B on the numerical solution of the magnetohydrodynamic equations, *J. Comp. Phys.*, *35*, 426, 1980.

Dorelli, J. C., A. Bhattacharjee, and J. Raeder, Separator reconnection at Earth's dayside magnetopause under generic northward interplanetary magnetic field conditions, *J. Geophys. Res.*, *112*, 1, doi:10.1029/2006JA011,877, 2007.

Evans, C. R., and J. F. Hawley, Simulation of magnetohydrodynamic flows: A constrained transport method, *Astrophys. J.*, *332*, 659, 1988.

Fedder, J. A., and J. G. Lyon, The solar wind - magnetosphere - ionosphere current - voltage relationship, *Geophys. Res. Lett.*, *14*, 880, 1987.

Finlay, C. C., et al., International geomagnetic reference field: the eleventh generation, *Geophysical Journal International*, *183*, 1216–1230, 2010.

Fuller-Rowell, T. J., D. Rees, S. Quegan, R. J. Moffett, M. V. Codrescu, and G. H. Millward, A coupled thermosphere-ionosphere model (CTIM), in *STEP Report*, edited by R. W. Schunk, p. 217, Scientific Committee on Solar Terrestrial Physics (SCOSTEP), NOAA/NGDC, Boulder, Colorado, 1996.

Ge, Y. S., J. Raeder, V. Angelopoulos, M. L. Gilson, and A. Runov, Interaction of dipolarization fronts within multiple bursty bulk flows in global MHD simulations of a substorm on 27 February 2009, *J. Geophys. Res.*, *116*, A00I23, 2011.

Harten, A., and G. Zwas, Self-adjusting hybrid schemes for shock computations, *J. Comput. Phys.*, *9*, 568, 1972.

Hirsch, C., *Numerical Computation of Internal and External Flow*, vol. II, John Wiley, New York, 1990.

Ijima, T., and T. A. Potemra, Field-aligned currents in the day side cusp observed by Triad, *J. Geophys. Res.*, *81*, 5971, 1976.

Kelley, M. C., *The Earth's Ionosphere*, Academic Press, New York, 1989.

Knight, S., Parallel electric fields, *Planet. Space Sci.*, *21*, 741, 1972.

Laney, C. B., *Computational Gasdynamics*, Cambridge University Press, 1998.

Le, G., J. Raeder, C. T. Russell, G. Lu, S. M. Petrinec, and F. S. Mozer, Polar cusp and vicinity under strongly northward IMF on April 11, 1997: Observations and MHD simulations, *J. Geophys. Res.*, *106*, 21,083, 2001.

Li, W., J. Raeder, J. C. Dorelli, M. Thomsen, and B. Lavraud, Solar wind entry into the magnetosphere under northward IMF conditions, *J. Geophys. Res.*, *113*, A04,204, 2008.

Li, W., J. Raeder, M. Øieroset, and T. D. Phan, Cold dense magnetopause boundary layer under northward IMF: Results from THEMIS and MHD simulations, *J. Geophys. Res.*, *114*, A00C15, doi:10.1029/2008JA013,497, 2009.

Li, W., J. Raeder, and D. Knipp, The relationship between dayside local Poynting flux enhancement and cusp reconnection, *J. Geophys. Res.*, *116*, A08,301, doi:10.1029/2011JA016,566, 2011.

Lui, A. T. Y., Extended consideration of a synthesis model for magnetic substorms, in *Magnetospheric Substorms*, edited by J. R. Kan, T. A. Potemra, S. Kokubun, and T. Ijima, vol. 64, p. 43, AGU Monogr. Ser., American Geophysical Union, 1991.

McPherron, R. L., Physical processes producing magnetospheric substorms and magnetic storms, in *Geomagnetism*, edited by J. Jacobs, vol. 4, p. 593, Academic Press, 1991.

McPherron, R. L., The role of substorms in the generation of magnetic storms, in *Magnetic Storms*, edited by B. T. Tsurutani, W. D. Gonzalez, Y. Kamide, and J. K. Arballo, vol. 98, p. 131, AGU Monogr. Ser., American Geophysical Union, 1997.

McPherron, R. L., C. T. Russell, and M. P. Aubry, Satellite studies of magnetospheric substorms on August 15, 1968, 9. Phenomenological model for substorms, *J. Geophys. Res.*, *78*, 3131, 1973.

Moretto, T., S. Vennerstrom, N. Olsen, L. Rastaetter, and J. Raeder, Using global magnetospheric models for simulation and interpretation of SWARM external field measurements, *Earth, Planets, Space*, *58*, 439–449, 2006.

Olsen, N., H. Lühr, T. J. Sabaka, M. Mandea, M. Rother, L. T. ffner Clausen, and S. Choi, CHAOS - a model of the Earth's magnetic field derived from CHAMP, Orsted, and SAC-C magnetic satellite data, *Geophys. J. Int.*, *166*, 67–75, 2006.

Pulkkinen, A., et al., Geospace environment modeling 2008-2009 challenge: Ground magnetic field perturbations, *Space Weather*, *9*, S02,004, 2011.

Pulkkinen, A., et al., Community-wide validation of geospace model ground magnetic field perturbation predictions to support model transition to operations, *Space Weather*, *11*, 369 doi:10.1002/swe.20,056, 2013.

Raeder, J., Global Magnetohydrodynamics – A Tutorial, in *Space Plasma Simulation*, edited by J. Büchner, C. T. Dum, and M. Scholer, Springer Verlag, Berlin Heidelberg New York, 2003.

Raeder, J., Flux transfer events: 1. Generation mechanism for strong southward IMF, *Ann. Geophys.*, *24*, 381, 2006.

Raeder, J., J. Berchem, and M. Ashour-Abdalla, The importance of small scale processes in global MHD simulations: Some numerical experiments, in *The Physics of Space Plasmas*, edited by T. Chang and J. R. Jasperse, vol. 14, p. 403, MIT Cent. for Theoret. Geo/Cosmo Plasma Phys., Cambridge, Mass., 1996.

Raeder, J., J. Berchem, and M. Ashour-Abdalla, The Geospace Environment Modeling grand challenge: Results from a Global Geospace Circulation Model, *J. Geophys. Res.*, *103*, 14,787, 1998.

Raeder, J., O. Vaisberg, V. Smirnov, and L. Avanov, Reconnection driven lobe convection: Interball tail probe observations and global simulations, *J. Atm. Solar-Terr. Phys.*, *62*, 833, 2000.

Raeder, J., Y. L. Wang, and T. J. Fuller-Rowell, Geomagnetic storm simulation with a coupled magnetosphere - ionosphere - thermosphere model, in *Space Weather, AGU Geophys. Monogr. Ser.*, edited by P. Song, G. Siscoe, and H. J. Singer, vol. 125, p. 377, American Geophysical Union, 2001a.

Raeder, J., Y. L. Wang, T. J. Fuller-Rowell, and H. J. Singer, Global simulation of space weather effects of the Bastille Day storm, *Sol. Phys.*, *204*, 325, 2001b.

Raeder, J., D. Larson, W. Li, E. L. Kepko, and T. Fuller-Rowell, OpenGGCM simulations for the THEMIS mission, *Space Sci. Rev.*, *141*, 535, 2008.

Raeder, J., P. Zhu, Y. Ge, and G. L. Siscoe, OpenGGCM simulation of a substorm: Axial tail instability and ballooning mode preceding substorm onset, *J. Geophys. Res.*, *115*, A00l16,

2010.

Raeder, J., P. Zhu, and Y. Ge, Auroral signatures of ballooning mode near substorm onset: OpenGGCM simulations, in *Auroral Phenomenology and Magnetospheric Processes: Earth and other Planets*, edited by A. Keiling, E. Donovan, F. Bagenal, and T. Karlsson, vol. 197 of *AGU Geophysical Monograph*, pp. 389–395, 2012.

Rastaetter, L., M. Hesse, M. Kuznetsova, J. B. Sigwarth, J. Raeder, and T. I. Gombosi, Polar cap size during 14-16 July 2000 (Bastille Day) solar coronal mass ejection event: MHD modeling and satellite imager observations, *J. Geophys. Res.*, *110*, A07,212, doi: 10.1029/2004JA010,672, 2005.

Rastatter, L., et al., Geospace Environment Modeling 2008-2009 challenge: Dst index, *Space Weather*, *11*, 187 doi:10.1002/swe.20,036, 2013.

Rishbeth, H., W. Deng, R. G. Roble, T. L. Killeen, and A. G. Burns, The flywheel effect: ionospheric currents after a geomagnetic storm, *Geophys. Res. Lett.*, *18*, 1845, 1991.

Ritter, P., H. Lühr, S. Maus, and A. Viljanen, High-latitude ionospheric currents during very quiet times: their characteristics and predictability, *Ann. Geophys.*, *22*, 2001, 2004.

Rostoker, G., Effects of substorms on the stormtime ring current index *Dst*, *Ann. Geophys.*, *18*, 1390–1398, 2000.

Russell, C. T., Y. L. Wang, and J. Raeder, The interplanetary shock of september 24, 1998: Arrival at Earth, *J. Geophys. Res.*, *105*, 25,143, 2001.

Sonnerup, B. U. O., and L. J. Cahill, Magnetopause structure and attitude from Explorer 12 observations, *J. Geophys. Res.*, *72*, 171, 1967.

Sonnerup, B. U. O., and L. J. Cahill, Explorer 12 observations of the magnetopause current layer, *J. Geophys. Res.*, *73*, 1757, 1968.

Strangeway, R. J., and J. Raeder, On the transition from collisionless to collisional magneto-hydrodynamics, *J. Geophys. Res.*, *106*, 1955, 2001.

Toth, G., The $\nabla \cdot B$ constraint in shock-capturing magnetohydrodynamics codes, *J. Comp. Phys.*, *161*, 605, 2000.

Vasyliunas, V. M., Mathematical models of magnetospheric convection and its coupling to the ionosphere, in *Particles and Fields in the Magnetosphere*, p. 61, Dordrecht, Netherlands: D. Reidel, 1970.

Vasyliunas, V. M., Electrodynamics of the ionosphere/magnetosphere/solar wind system at high latitudes, in *NATO Advanced Studies Inst.*, Lillehammer, 1988.

Vennerstrom, S., T. Moretto, L. Rastaetter, and J. Raeder, Field-aligned currents during northward interplanetary field: Morphology and causes, *J. Geophys. Res.*, *110*, A06,205, doi: 10.1029/2004JA010,802, 2005.

Vennerstrom, S., T. Moretto, L. Rastaetter, and J. Raeder, Modeling and analysis of solar wind generated contributions to the near-Earth magnetic field, *Earth, Planets, Space*, *58*, 451–461, 2006.

Weimer, D. R., An improved model of ionospheric electric potentials including substorm perturbations and application to the Geospace Environment Modeling November 24, 1996, event, *J. Geophys. Res.*, *106*, 407, 2001.

Wolf, R. A., The quasi-static (slow flow) region of the magnetosphere, in *Solar Terrestrial Physics*, edited by R. L. Carovillano and J. M. Forbes, p. 303, D. Reidel, Hingham, MA, 1983.

Zalesak, S. T., Fully multidimensional flux-corrected transport, *J. Comp. Phys.*, *31*, 355, 1979.

Zalesak, S. T., Very high order pseudospectral flux-corrected transport (FCT) algorithms for conservation laws, in *Proceedings of the Fourth IMACS International Symposium on Computer Methods for Partial Differential Equations*, edited by R. Vichnevetsky and R. S. Stepleman, p. 126, IMACS, Rutgers University, New Brunswick, 1981.

Zhu, P., J. Raeder, C. C. Hegna, and C. R. Sovinec, Nature of axial tail instability and bubble-blob formation in near-Earth plasma sheet, *J. Geophys. Res.*, *118*, 1–11 doi:10.1029/2012JA017,972, 2013.